http://dx.doi.org/10.21577/0103-5053.20170154

J. Braz. Chem. Soc., Vol. 29, No. 2, 404-411, 2018.
Printed in Brazil - ©2018 Sociedade Brasileira de Química

Article

Thermal Properties and Kinetics of Al/α-MnO_2 Nanostructure Thermite

Jia-Xing Song,[a] Xiang Fang,[a] Tao Guo,[a] Feng-Li Bei,[b] Wen Ding,[a] Xiao-Nan Zhang,[,a] Miao Yao[a] and Hong-Jun Yu[b]*

[a]*College of Field Engineering, PLA University of Science and Technology, 210007 Nanjing, China*

[b]*School of Chemical Engineering, Nanjing University of Science and Technology, 210094 Nanjing, China*

In this work, thermal properties and kinetics of Al-nanoparticles/α-MnO_2 nanorods thermite were reported. The α-MnO_2 nanorods were synthesized using a hydrothermal method and were characterized by X-ray powder diffraction (XRD) and X-ray photoelectron spectra (XPS), then combined with Al nanoparticles based on the ultrasonic mixing method to prepare the nanostructure thermite. Besides, both pure components and mixture were characterized by field emission scanning electron microscopy (FE-SEM) to observe their morphologies and structures. Subsequently, the thermal properties of Al/α-MnO_2 nanostructure thermite were studied on the basis of thermogravimetric-differential scanning calorimetry (TG-DSC). According to the TG-DSC tests, the calculation results of activation energy for kinetics of Al/α-MnO_2 thermite were obtained using different isoconversional methods. It was found that Al/α-MnO_2 nanostructure thermite has high heat release and low onset temperature, and the heat release of the nanostructure thermite was approximately 1146.6 J g^{-1}.

Keywords: Al/α-MnO_2 thermite, thermal properties, isoconversional method

Introduction

Thermites, as one of the traditional energetic materials, store high amount of chemical energy that could be released rapidly through the oxidation-reduction reaction called thermite reaction. Thermite reaction is considered to generate molten metal and release plentiful heat from exothermic thermite mixture or composites.[1-3] As a type of oxidation-reduction reaction, molten metal can be produced when the fuel reduces the metallic oxide:[4]

$$A + MO = AO + M + \Delta H \quad (1)$$

where A is the fuel, usually aluminum (Al) or magnesium (Mg). ΔH is the heat of reaction, and MO is the metallic oxide, such as CuO, Fe_2O_3, MnO_2, SiO_2 and MoO_3.[5-9] Among such metallic oxides, as oxidizing agent in thermite system, the manganese dioxide is one of the high energy materials with high heat release but lack of research.[9,10]

In recent years, an increasing number of researchers pay much attention to nano-materials preparations and nano-thermite properties based on the rapid development of techniques. The Al/Fe_2O_3 nano-thermites have attracted extensive attention from scholars. For example, Wang *et al.*[11] investigated the mechanism for thermite reactions of Al/Fe_2O_3 nanocomposites on the basis of residue analysis. Through using X-ray powder diffraction (XRD) to analyze the specific products, they speculate the most reasonable equations from the possible reactions in accordance with the minimum free energy principle. In addition, various shapes of nano-Fe_2O_3 are synthesized to prepare thermite system with Al, for example, pollen-like Fe_2O_3/Al thermite[6] and Fe_2O_3 nanorods/Al thermite.[12] The thermal properties of such Fe_2O_3/Al thermites are also studied. The results show that nano-thermites have superior heat release characteristics. CuO is also the common metallic oxide added into thermite. The effects of particle size and agglomeration of CuO on the thermal behavior and ignition kinetics of Mg-CuO thermite systems are investigated.[13] The activation energies for the Mg-CuO thermite systems are estimated by applying isoconversional method. Besides, CuO nanowires, with diameter about 30-100 nm and length about 15 μm, are synthesized with the application of a vapor-phase approach.[14] Then, the CuO nanowires are coated with Al nanoparticles by radio-frequency sputtering, which are studied as nanoenergetic materials in comparison with the mixture of CuO and Al nanopowders. Based on the thermogravimetric-differential scanning calorimetry (TG-DSC) analysis, the

*e-mail: 1023855857@qq.com

nanoenergetic materials have higher exothermic peak and heat than the mixture due to more intimate contact and lower oxidation level.[15]

According to Fischer's[16] research, reaction heat of $4Al + 3MnO_2$ is higher than both $2Al + 3CuO$ and $2Al + Fe_2O_3$, which could be used in explosives, pyrotechnics, compositions, propellants and fuels preferably. As for MnO_2, the estimation of isothermal values of activation energy for micron level MnO_2-Al aluminothermic reduction was reported at an early stage,[17] but the molar ratio of MnO_2 and Al was about 1:5. In fact, the molar ratio of MnO_2 and Al should be about 3:4 on the basis of chemical equation. Recently, Meeks *et al.*[18] researched the effects of rheological properties on the reactivity of energetic thin films with the selection of Mg as fuel. Both powdered Mg and MnO_2 were micron sized particles sieved to a 325 mesh. Compared with Mg, Al was more secure and stable.[19] As for nano-MnO_2, numerous researchers focus on its magnetic properties and capacitive behavior rather than the thermal properties.[20-24] In this work, we focus on the thermal properties and kinetics of the Al/MnO_2 nanostructure thermite.

The activation energy of thermites is an important parameter to the reaction kinetics. Such activation energy is defined as the minimum amount of energy required to initiate the reaction between the thermite constituents.[25] Isoconversional methods are widely used in processing data to obtain the value of activation energy at present. Isoconversional methods can determine E_a (activation energy) without the knowledge or assumption of kinetics model and can reveal the dependence of E_a on conversion α.[26,27] The Kissinger-Akahira-Sunose (KAS) method is one of the most famous isoconversional methods on behalf of differential method to determine activation energy.[28,29] For the integration method, Vyazovkin advanced isoconversional method can be used to obtain the reliable activation energy.[30,31] Thus, we choose both isoconversional methods, KAS and Vyazovkin methods, to try to calculate the activation energy of the Al/MnO_2 nanostructure thermite.

To the best of our knowledge, few articles have been published concerning the thermal properties and kinetics of the Al/MnO_2 nanostructure thermite, especially MnO_2 nanorods. Therefore, this paper attempted to study the thermal properties and kinetics of Al/MnO_2 nanostructure thermite. MnO_2 nanorods were synthesized by using potassium permanganate ($KMnO_4$) and diluted hydrochloric acid (HCl) based on hydrothermal method[20] and characterized by XRD, X-ray photoelectron spectra (XPS) and field emission scanning electron microscopy (FE-SEM). The ultrasonic mixing method, as the most commonly used method, was chosen to prepare the Al/α-MnO_2 nanostructure thermite. Subsequently, the fabricated thermite mixture was characterized by FE-SEM and TG-DSC, and we studied the onset temperature, peak temperature and heat released of the Al/α-MnO_2 nanostructure thermite. Then, according to the TG-DSC tests, the E_a of the Al/α-MnO_2 nanostructure thermite was obtained through KAS isoconversional method. And the changes of E_a on extent of conversion (α) for kinetics of Al/α-MnO_2 thermite were obtained by using IsoKin Isoconversional Data Analysis Program version 1.42 based on Vyazovkin isoconversional method. In the end, the calculation results of two methods were discussed.

Experimental

Materials

All chemicals were analytical reagent grade and were used without any further treatment or purification. Both $KMnO_4$ and HCl were supplied by Lingfeng chemical reagent Co., LTD. (Shanghai, China). In addition, the nano-Al fuel with 100 nm average diameter was purchased from Aladdin Industrial Corporation (Shanghai, China).

α-MnO_2 preparation

The α-MnO_2 was prepared via a hydrothermal method as follows: 5 g $KMnO_4$ was dissolved into 50 mL deionized water, which was stirred intensely through the magnetic stirring apparatus for about 10 min. Then, 3.75 mL HCl was extracted by pipette and diluted with 20 mL deionized water. Besides, the diluted HCl solution was added dropwise into the stirring $KMnO_4$ solution. After that, the mixture solution was then transferred into a 100 mL Teflon-lined stainless steel autoclave, sealed and maintained at 140 °C for 12 h in an electric oven. When the autoclave was cooled to the room temperature, we took out the product, which was a dark brown granule. The obtained powder was washed for several times with deionized water and ethyl alcohol. After the centrifugal operation, the product was dried at 60 °C for 12 h.

The chemical reactions involved in the synthesis of the α-MnO_2 were as follows:[20]

When HCl is excessive, the $MnCl_2$ solution is obtained:

$$2KMnO_4 + 16HCl \rightarrow 2KCl + 2MnCl_2 + 5Cl_2 + 8H_2O \quad (2)$$

But, if theHCl concentration is low, $MnCl_2$ will be oxidized to the MnO_2 precipitation:

$$2KMnO_4 + 3MnCl_2 + 2H_2O \rightarrow 2KCl + 5MnO_2\downarrow + 4HCl \quad (3)$$

Sample preparation

In this paper, the nanostructure thermite of Al and α-MnO_2 was prepared through the use of ultrasonic mixing method. Prior to the mixing process, 5.00 g Al and 2.14 g α-MnO_2 (molar ratio of MnO_2-Al about 3:7) were immersed in cyclohexane with magnetic stirring for 30 min separately. Then, both mixed liquids were sonicated for 30 min primarily in a sonic bath (Hechuang, KH3200E). Next, the cyclohexane solution of Al was slowly and homogeneously added into the cyclohexane solution of α-MnO_2. The suspension was ultrasonic dispersed and magnetic agitated for several times until the cyclohexane was almost evaporated to dryness under ambient condition. After ultrasonic mixing operation, the slurry was dried at 60 °C for 12 h under vacuum environment.

Characterization analysis

The prepared α-MnO_2 sample phase and chemical composition was characterized by using the XRD analysis (Bruker, D8 Advance, Germany) and XPS analysis (Escalab 250Xi, USA). The morphologies, particle size and mixing quality of the materials and mixture were characterized by field emission scanning electron microscope (FE-SEM) analysis (HITACHI High-Technologies corporation, S-4800 II, Japan).

Thermal analysis

The investigation of thermal behavior was carried out based on the TG-DSC (NETZSCH STA 449F3, Germany) analysis. The sample mass was about 15 mg and the heating rates were 8, 10, 12, 14 °C min^{-1} in corundum crucible, covering the temperature range from room temperature to 1000 °C in nitrogen atmosphere.

Theoretical background

The KAS isoconversional method, one of the most reliable model-free isoconversional methods for the calculation of activation energy for thermite reaction, was used to determine the activation energy of the kinetics of Al/α-MnO_2 nanostructure thermite in this work.[26-29] The KAS isoconversional method can be expressed through the following equation:

$$\ln\left(\frac{\beta}{T^2}\right) = \ln\left(\frac{AR}{E_a g(\alpha)}\right) - \frac{E_a}{RT} \quad (4)$$

where α is the degree of conversion, β the linear heating rate (°C min^{-1}), T the absolute temperature (K), R the universal gas constant (J mol^{-1} K^{-1}), A the pre-exponential factor (s^{-1}) and E_a is the activation energy (kJ mol^{-1}). Assuming that the rate of reaction reaches maximum at the peak temperature, the plot of ln (β/T^2) *vs.* 1/T should be a straight line whose slope can be used to evaluate the activation energy E_a.

The Vyazovkin advanced isoconversional method does not require model assumption based on the integral equation of the dynamic parameter.[30,31] For the non-isothermal solidification process of linear temperature rise, the Vyazovkin advanced isoconversional method can be expressed through the following equation:

$$\sum_{i}^{n}\sum_{j\neq i}^{n} J[E_a, T_i(t)] / J[E_a, T_j(t)] = \text{minimum} \quad (5)$$

$$J[E, T(t)] = \int_0^t \exp[-E / RT(t)]dt \quad (6)$$

where J is the temperature integral, $T_i(t)$ (I = 1,…, n) are actual temperature variations, n the number of test, i and j representing the test results of different heating processes.

Results and Discussion

Results of XRD analysis

Figure 1 presents the XRD patterns of the obtained products. Compared with a tetragonal α-MnO_2 phase (ICDD/JCPDS 44-0141 MDI Jade 6.0), the matching degree is pretty high. As shown in Figure 1, no distinct anomalous peaks can be found, indicating the really high purity of the obtained product. The lattice constants are a = 9.785 Å, c = 2.863 Å, c/a = 0.293 and space group is I4/m.

Results of XPS analysis

Figure 2 shows a survey spectrum of the MnO_2 sample. We can see that the most intense peaks in the spectrum are those of oxygen (O) and manganese (Mn). The peak of potassium (K) has surprisingly low intensity because of the raw material $KMnO_4$. The peak details are listed in Table 1. It can be seen that the peak of Mn-2p is 642.44 eV. According to the XPS spectrum data, the valence state of Mn is (+4). In the listing of atomic%, the content of O-1s is about 50.81%, and the content of Mn-2p is about 22.95%.

Results of FE-SEM analysis

Figure 3 shows FE-SEM image of the pure components. The overall appearance of the α-MnO_2 nanorods is depicted in Figure 3a; the nanorods are randomly distributed

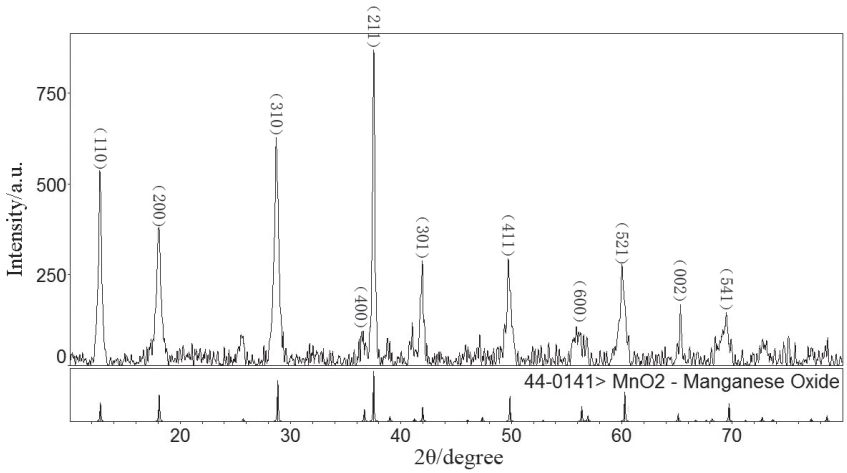

Figure 1. XRD patterns of the obtained products.

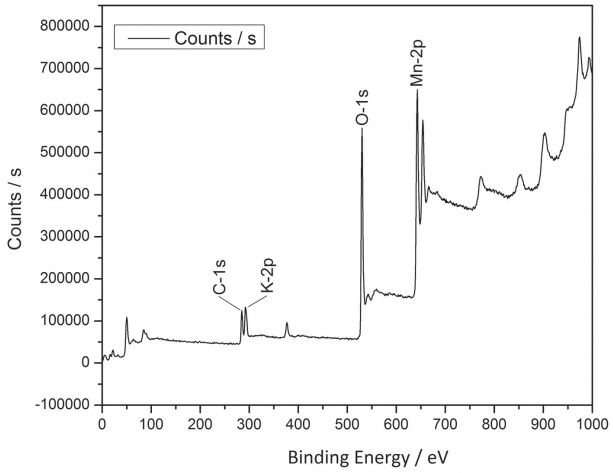

Figure 2. Survey XPS of the MnO_2 sample.

evenly on the surface with variety of length and thickness. According to Figure 3b, the nanorods have smooth surfaces, and the structures are integrated. As for thickness, the diameter of α-MnO_2 nanorods ranges from 40 to 100 nm. Besides, Figure 3c shows the spherical morphology of the Al nanoparticles and diameter of the Al spheres ranges from 50 to 250 nm.

Figure 4 shows FE-SEM image of the Al/α-MnO_2 nanostructure thermite prepared by ultrasonic mixing method and the α-MnO_2 nanorods and Al nanoparticles are dispersed relatively evenly. Besides, in the picture of local details of the thermite, several Al nanoparticles adhere to the surface of α-MnO_2 nanorods, which can be found in Figure 4b. However, unavoidable agglomerations[32] of Al nanoparticles could be found. The large size agglomerates

Table 1. Details of peaks in the survey spectrum

Name	Start BE / eV	Peak BE / eV	End BE / eV	Atomic%
C-1s	291.03	284.79	279.98	20.24
K-2p	305.88	292.03	287.98	6.00
O-1s	545.88	529.83	525.98	50.81
Mn-2p	664.88	642.44	632.98	22.95

BE: binding energy.

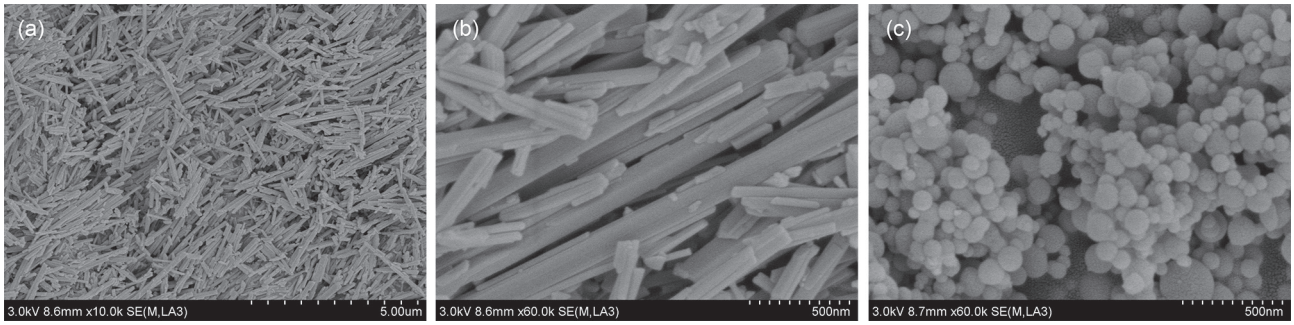

Figure 3. FE-SEM images of (a) pure α-MnO_2 nanorods; (b) size of nanorods and (c) Al nanoparticles.

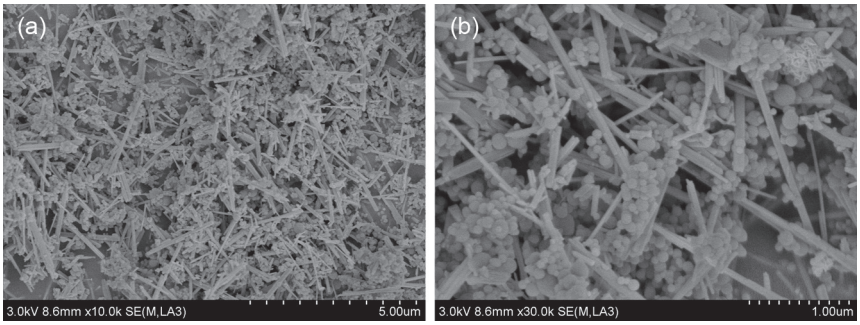

Figure 4. FE-SEM images of (a) the Al/α-MnO_2 nanostructure thermite and (b) the local details of the thermite.

may never ignite or ignite after very long delays. Due to delayed ignition, such agglomerates cannot often burn during the limited time.[13] Thus, a large portion of the particles remains unburned, dramatically reducing the efficiency of the system.[33] Besides, agglomeration can increase the diffusion distance between fuel and oxide. As a result, it has definitely adverse effects on heat release and ignition. Agglomeration has imposed a vital influence on the measurement of heat release. However, the good thing is no particularly huge agglomeration can be seen in the FE-SEM image, which will relatively reduce the adverse effects on heat release.

Thermal properties analysis

Figure 5 shows the TG-DSC curves of Al/α-MnO_2 nanostructure thermite samples. In order to research the thermal properties of the sample, the onset temperature, peak temperature and heat release during TG-DSC tests were studied and the mass changes of TG curves at different heating rates were listed in Table 2. In addition, ΔM_{150}, $\Delta M_{150\text{-}300}$, $\Delta M_{500\text{-}750}$ and $\Delta M_{750\text{-}900}$ mean the mass change at the range of temperature from room temperature to 150 °C, 150 to 300 °C, 500 to 750 °C and 750 to 900 °C, respectively. Consequently, the change of mass in Figure 5a is the average of four tests at different heating rates.

According to Figure 5a and Table 2, there is a slight mass loss (ΔM_{150} about 1.63%) in all of the TG curves roughly ranging from room temperature to 150 °C due to desorption of H_2O and cyclohexane on the surface of Al/α-MnO_2 nanostructure thermite. Since MnO_2 is well known for its ability to adsorb water,[34] the initial mass loss up to 150 °C is due to the removal of physisorbed water. And some residual cyclohexane was desorbed from the surface in the meantime.[35] Then, the second mass loss ($\Delta M_{150\text{-}300}$ about 2.14%) in region from 150 to 300 °C relates to the removal of structural water from α-MnO_2 nanorods.[36] With the application of hydrothermal method, the water structure could exist in the structure of the α-MnO_2 nanorods.

After the mass loss below 300 °C, no significant mass loss or mass gain can be found at the range of temperature from 300 to 600 °C. The thermite reaction, meaning oxygen transfer from the MnO_2 to the Al should not exhibit any change in the mass signal due to conservation of mass. Besides, the thermite reaction is explained by the heat release signal. In Figure 5b, there is an apparently main

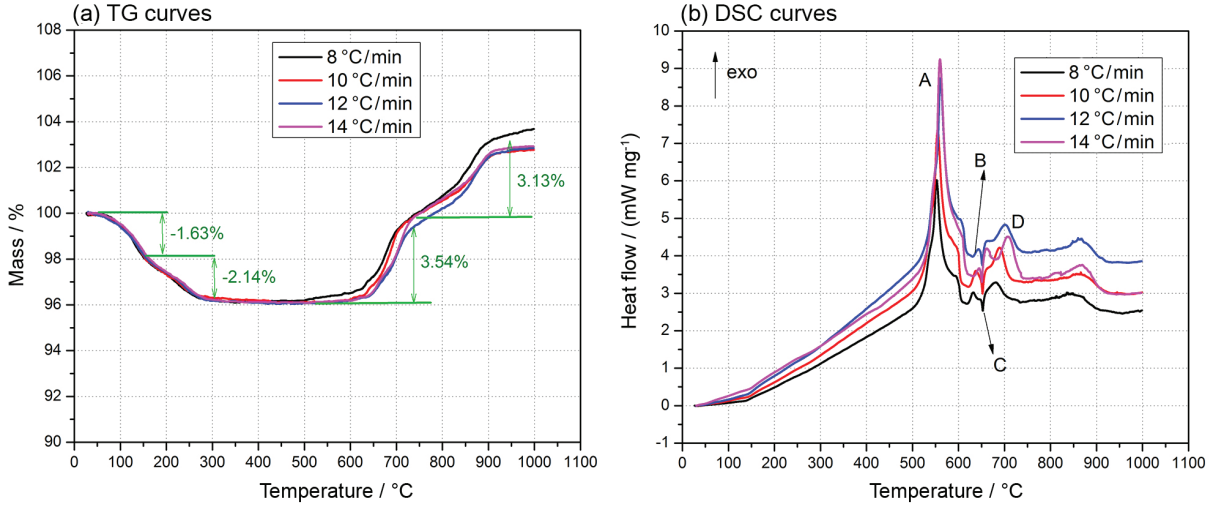

Figure 5. TG-DSC curves of Al/α-MnO_2 nanostructure thermite.

Table 2. The mass changes of Al/α-MnO_2 nanostructure thermite in TG curves

Heating rate	8 °C min^{-1}	10 °C min^{-1}	12 °C min^{-1}	14 °C min^{-1}	Average
ΔM_{150} / %	–1.92	–1.43	–2.21	–0.94	–1.63
$\Delta M_{150\text{-}300}$ / %	–1.88	–2.19	–1.65	–2.83	–2.14
$\Delta M_{500\text{-}750}$ / %	3.17	3.71	3.56	3.73	3.54
$\Delta M_{750\text{-}900}$ / %	3.87	2.77	2.99	2.89	3.13

ΔM_{150}: the mass change at the range of temperature from room temperature to 150 °C; $\Delta M_{150\text{-}300}$: the mass change at the range of temperature from 150 to 300 °C; $\Delta M_{500\text{-}750}$: the mass change at the range of temperature from 500 to 750 °C; $\Delta M_{750\text{-}900}$: the mass change at the range of temperature from 750 to 900 °C.

Table 3. DSC parameters of Al/α-MnO_2 nanostructure thermite

Heating rate	8 °C min^{-1}	10 °C min^{-1}	12 °C min^{-1}	14 °C min^{-1}	Average
Heat release / (J g^{-1})	1113.2	1137.3	1151.3	1184.5	1146.6
Onset temperature / °C	541.7	541.6	545.9	548.4	544.4
Peak temperature / °C	552.6	554.7	556.9	559.6	555.9
End temperature / °C	560.1	560.4	567.2	569.6	564.3
Peak height / (mW mg^{-1})	3.325	4.251	4.879	5.768	–

exothermic peak in each different DSC curve from 500 to 600 °C. Besides, the details of the main exothermic peaks at different heating rates were listed in Table 3. The DSC curves show that as the heating rate is increased, the peak temperature (point A) is shifted to higher temperature. On the basis of DSC curves, the onset temperature is near 544 °C and the end temperature is near 564 °C, which are lower than the melting point of Al. The peak temperature (point A) is near 556 °C, indicating that the solid Al nanoparticles reacting with MnO_2 is the first priority and the heat release of the Al/α-MnO_2 nanostructure thermite is measured about 1146.6 J g^{-1}. The performances of the nano materials are active and large interfacial contact area between Al nanoparticles and α-MnO_2 nanorods provides more active sites for achieving sufficient reaction. Due to more intimate contact and catalytic function of α-MnO_2 nanorods, the Al/α-MnO_2 nanostructure thermite could have high heat release and low onset temperature.

Finally, there are two apparent mass gain (about 3.5 and 3.13%) in the TG curves roughly from 600 to 900 °C. Since the TG-DSC is run in the nitrogen atmosphere and the mass gain is due to the reaction of the Al to nitrogen in the environment, aluminum nitride (AlN) is produced, releasing part of the heat.[37] After the main heat release signal in Figure 5b, there are two relatively small exothermic peaks (points B and D) and a small endothermic peak (point C). Besides, the small endothermic peak (point C) represents the melting point of Al.

Activation energy

Potential hazards associated with the thermal properties of energetic materials require that stability evaluation and ignition kinetics be carried out to assure the safe processing, handling and storage.[38] Based upon KAS isoconversional method mentioned in equation 4, the plot of ln (β/T^2) *vs.* 1/T at the peak temperature was constructed in Figure 6. The analytical expression of the data correlation line was Y = –53074X + 52.951. The correlation coefficient R was about –0.9899, and the activation energy E_a, deduced from the slope of the data correlation line, was about 440 kJ mol^{-1}, which is due to the activation energy of the fastest reaction at peak temperature.

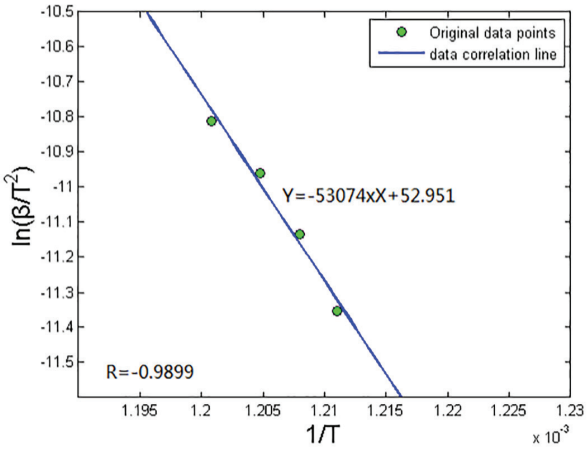

Figure 6. The data correlation line of ln (β/T^2) *vs.* 1/T.

In order to make a comparison with the calculation result of KAS method, the Vyazovkin advanced isoconversional method mentioned in equation 5 was applied to obtain the dependence of E_a on conversion (α) for Al/α-MnO_2 nanostructure thermite by using IsoKin Isoconversional Data Analysis Program version 1.42 (Center for Thermal Analysis, University of Ultra), as shown in Figure 7. The error bars

shown in Figure 7 represented error limits corresponding to 95% confidence interval. As can be seen, E_a has a high dependence on α during the reaction. At the beginning of the reaction, the thermal energy barrier is relatively small. As the reaction continues, the thermal energy barrier becomes higher in the conversion range of $0.05 \leq \alpha \leq 0.45$. As shown in Zone 1, the activation energy varied from 198 to 343 kJ mol^{-1}. However, in Zone 2, the activation energy is falling slowly from 216 to 153 kJ mol^{-1} in the conversion range of $0.55 \leq \alpha \leq 0.95$. Besides, there is a distinct bluff between Zone 1 and Zone 2. Namely, the reaction mechanisms of Al/α-MnO_2 nanostructure thermite reaction have two processes and at least two mechanism functions.

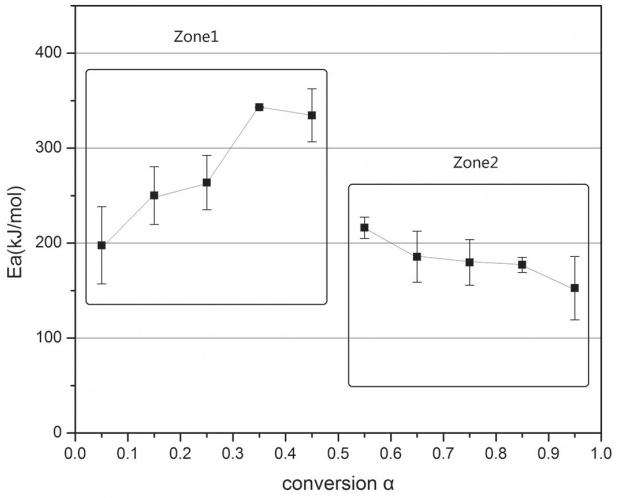

Figure 7. Changes of activation energy (E_a) on the degree of conversion (α).

Comparing with the result of KAS isoconversional method, the values of activation energy E_a calculated by Vyazovkin advanced isoconversional method are relatively less than that of KAS isoconversional method. According to previous studies,[29-31] in the hypothesis of KAS method, the peak temperature represents the fastest reaction rate. Also, there is a certain error in the hypothesis leading to the high computation of activation energy, which makes the error of KAS method relatively major. Besides, the TG-DSC test instrument also has a certain systematic error.

Conclusions

In this study, the thermal properties and kinetics of the Al/α-MnO_2 nanostructure thermite were investigated by using XRD, XPS, FE-SEM and TG-DSC techniques. The α-MnO_2 nanorods could be synthesized by hydrothermal method effectively. The mixture of Al/α-MnO_2 nanostructure thermite is relatively uniform via ultrasonic method. But the agglomeration was one of the unavoidable and universal phenomena in nano-materials. Based on the result of the TG-DSC experiment, the thermite reactions between Al nanoparticles and MnO_2 nanorods happened before the Al nanoparticles melted. The thermite reaction occurred at the solid phase. The onset temperature was near 544 °C and the heat release of Al/α-MnO_2 nanostructure thermite measured was about 1146.6 J g^{-1}. Due to more intimate contact and catalytic function of α-MnO_2 nanorods, the Al/α-MnO_2 nanostructure thermite had high heat release and low onset temperature. Finally, the activation energy E_a of Al/α-MnO_2 nanostructure thermite was estimated by applying KAS method and Vyazovkin advanced isoconversional method. The calculation results of KAS method is higher than that of Vyazovkin method, but still has reference value to some extent. The E_a *vs.* α curve indicated that the activation energies increased in the conversion range of $0.05 \leq \alpha \leq 0.45$ while the activation energies decreased in the conversion range of $0.55 \leq \alpha \leq 0.95$. It was also revealed that the different mechanisms of Al/α-MnO_2 nanostructure thermite during the reaction.

Acknowledgments

This work was supported by the National Natural Science Foundation, project No. 51673213 and No. 51505498. It was performed using the equipment at the School of Chemical Engineering at Nanjing University of Science and Technology (NUST).

References

1. Wang, L. L.; Munir, Z. A.; Maximov, Y. M.; *J. Mater. Sci.* **1993**, *28*, 3693.
2. Zhu, H. G.; Wu, S. Q.; Wang, H. Z.; *Chin. J. Nonferrous Met.* **2001**, *12*, 382.
3. Bazyn, T.; Lynch, P.; Krier, H.; *Propellants, Explos. Pyrotech.* **2010**, *35*, 93.
4. Kinsey, A. H.; Slusarski, K.; Woll, K.; Gibbins, D.; Weihs, T. P.; *J. Mater. Sci.* **2016**, *51*, 5738.
5. Park, Y.; Seo, S.; Jang, S.; Choi, H.; Park, J. S.; *Combust. Sci. Technol.* **2016**, *6*, 895.
6. Hu, X. L.; Liao, X.; Xiao, L. Q.; Jian, X. X.; Zhou, W. L.; *Propellants, Explos., Pyrotech.* **2015**, *40*, 867.
7. Bacciochini, A.; Radulescu, M. I.; Yandouzi, M.; Maines, G.; Lee, J. J.; Jodoin, B.; *Surf. Coat. Technol.* **2013**, *226*, 60.
8. Delgado, A.; Cordova, S.; Shafirovich, E.; *Combust. Flame* **2015**, *162*, 3333.
9. Fischer, S. H.; Grubelich, M. C.; *Aiaa J.* **1996**, DOI: 10.2514/6.1996-3018.
10. Rossi, C.; Zhang, K.; Esteve, D.; Alphonse, P.; Tailhades, P.; Vahlas, C.; *J. Microelectromech. Syst.* **2007**, *16*, 919.

11. Wang, Y.; Song, X. L.; Jiang, W.; Deng, G. D.; Guo, X. D.; Liu, H. Y.; Li, F. S.; *Trans. Nonferrous Met. Soc. China* **2014**, *24*, 263.
12. Zhao, N. N.; He, C. C.; Liu, J. B.; Ma, H. X.; An, T.; Zhao, F. Q.; *Acta Phys. Chim. Sin.* **2013**, *29*, 2498.
13. Hosseini, S. G.; Sheikhpour, A.; Keshavarz, M. H.; Tavangar, S.; *Thermochim. Acta* **2016**, *626*, 1.
14. Jiang, X. C.; Herricks, T.; Xia, Y. N.; *Nano Lett.* **2002**, *2*, 1333.
15. Kim, D. K.; Bae, J. H.; Kang, M. K.; Kim, H. J.; *Curr. Appl. Phys*. **2011**, *11*, 1067.
16. Fischer, S. H.; Grubelich, M. C.; *Sandia Natl. Lab. [Tech. Rep.] SAND* **1996**, SAND--96-1795C. Available at https://www.osti.gov/scitech/servlets/purl/372668, accessed in August 2017.
17. Sarangi, B.; Ray, H. S.; Dash, R. R.; *Metall. Mater. Trans. B* **1998**, *29*, 1135.
18. Meeks, K. A.; Clark, B. R.; Cano, J. E.; Apblett, C. A.; Pantoya, M. L.; *Combust. Flame* **2015**, *162*, 3288.
19. Trunov, M. A.; Schoenitz, M.; Dreizin, E. L.; *Propellants, Explos., Pyrotech.* **2005**, *30*, 36.
20. Xu, R. R.; Pang, W. Q.; *Inorganic Synthesis and Preparation Chemistry*; Higher Education Press: Beijing, China, 2012.
21. Zhao, J. G.; Yin, J. Z.; Yang, S. G.; *Mater. Res. Bull*. **2012**, *47*, 896.
22. Dreizin, E. L.; *Prog. Energy Combust. Sci.* **2009**, *35*, 141.
23. Deng, M. G.; Chen, Y. F.; *Adv. Mater. Res*. **2011**, *14*, 152.
24. Singh, I. B.; Park, S. M.; *Indian J. Chem*. **2015**, *54*, 45.
25. Cervantes, O. G.; Kuntz, J. D.; Gash, A. E.; Munir, Z. A.; *Combust. Flame* **2011**, *158*, 117.
26. Kissniger, H. E.; *J. Res. Natl. Bur. Stand.* **1956**, *57*, 217.
27. Badiola, C.; Schoenitz, M.; Zhu, X.; Dreizin, E. L.; *J. Alloys Compd.* **2009**, *488*, 386.
28. Mostaan, H.; Karimzadeh, F.; Abbasi M. H.; *Thermochim. Acta* **2010**, *511*, 32.
29. Kissniger, H. E.; *Anal. Chem.* **1957**, *29*, 1702.
30. Vyazovkin, S.; *J. Comput. Chem.* **1998**, *18*, 393.
31. Vyazovkin, S.; *J. Therm. Anal.* **1997**, *49*, 1493.
32. Singhal, A.; Skandan, G.; Wang, A.; Glumac, N.; Kear, B. H.; Hunt, R. D.; *Nanostruct. Mater.* **1999**, *11*, 545.
33. Dreizin, E. L.; *Prog. Energy Combust. Sci*. **2009**, *35*, 141.
34. Fraioli, A. V.; *Proc. Electrochem. Soc*. **1985**, *85*, 342.
35. Williams, R. A.; Schoenitz, M.; Ermoline, A.; Dreizin, E. L.; *Thermochim. Acta* **2014**, *594*, 1.
36. Wesley, M. D.; Scott, W. D.; *Mater. Sci. Eng. B* **2011**, *176*, 1169.
37. Sakurai, T.; Yamada, O.; Miyamoto, Y.; *Mater. Sci. Eng. A* **2006**, *415*, 40.
38. Eslami, A.; Hosseini, S. G.; *J. Therm. Anal. Calorim.* **2011**, *104*, 671.

Submitted: June 18, 2017
Published online: August 29, 2017